USGS
science for a changing world

Analysis of MASTER Thermal Data in the Greeley Area of the Front Range Urban Corridor, Colorado—Delineation of Sites for Infrastructure Resource Characterization

U.S. Geological Survey Bulletin 2196

U.S. Department of the Interior
U.S. Geological Survey

Analysis of MASTER Thermal Data in the Greeley Area of the Front Range Urban Corridor, Colorado—Delineation of Sites for Infrastructure Resource Characterization

By K. Eric Livo *and* Ken Watson

U.S. Geological Survey Bulletin 2196

U.S. Department of the Interior
U.S. Geological Survey

U.S. Department of the Interior
Gale A. Norton, Secretary

U.S. Geological Survey
Charles G. Groat, Director

U.S. Geological Survey, Reston, Virginia: 2004

This report is only available on-line at: http://pubs.usgs.gov/bul/b2196

For more information about the USGS and its products:
Telephone: 1-888-ASK-USGS
World Wide Web: http://www.usgs.gov/

Contents

Figures

Tables

Analysis of MASTER Thermal Data in the Greeley Area of the Front Range Urban Corridor, Colorado—Delineation of Sites for Infrastructure Resource Characterization

By K. Eric Livo *and* Ken Watson

Abstract

Sand and soils southwest of Greeley, Colorado, were characterized for mineral composition and industrial quality. Radiance data from the thermal channels of the MASTER simulator were calibrated using estimated atmospheric parameters. Channel emissivities were approximated using an estimated ground temperature. Subsequently, a decorrelation algorithm was used to calculate inverse wave emissivity images. Six soil classes, one vegetation class, water, and several small classes were defined using an unsupervised classification algorithm. Ground covered by each of the derived emissivity spectral classes was studied using color-infrared air photos, color-infrared composite MASTER data, geologic maps, NASA/JPL Airborne Visible and Infrared Imaging Spectrometer (AVIRIS) data, and field examination.

Spectral classes were characterized by their responses and related to their mineral content through field examination. Classes with a minimum at channel 44, and having a similar spectral shape to quartz, field checked as containing abundant quartz. Classes with a minimum at channel 45, and having a spectral shape similar to the sheet minerals, were found in the field to contain abundant mica and clay. Sandy soil was found to have a positive slope at the longer wavelengths; the more clay rich soils had a negative slope. Spectra with a strong downturn at channel 50 generally indicated low vegetation cover, whereas an upturn indicated more vegetation cover.

Mapping revealed a range of classified soils with varying amounts of quartz, silt, clay, and plant humus. Sand and gravel operations along the St. Vrain River, gravel lots, and some fields spectrally classified as quartz-rich sands were confirmed through field examination. Other fields mapped as sandy soils, ranging from quartz-rich sandy soil to quartz-rich silt-sand soil with clay. Flood plains mapped as sandy-silty-organic-rich clay.

The city of Greeley contained all classes of materials, with the sand classes mapping as various types of asphalt. Abundant quartz gravel was apparent within the asphalt during field checking. The clay classes mapped silt-clay soils in areas of irrigated grass landscaping, some fields, and roofing materials.

Introduction

An important focus of current studies in the U.S. Geological Survey National Infrastructure Project is the characterization of the mineral composition and industrial quality of construction materials, particularly sand and gravel deposits. One of the areas chosen for this investigation is the Front Range Urban Corridor of Colorado. This study focuses on data acquired along the South Platte and St. Vrain River drainage from Denver to Greeley, Colo. Remotely sensed data, primarily multispectral thermal infrared, supplemented with broadband reflectance data for vegetation information and reflectance imaging spectroscopy data for mica and clay identification, were used in the study.

The thermal-infrared (TIR) region of the electromagnetic spectrum (3–35 μm) contains diagnostic spectral features of the most common rock-forming minerals (fig. 1) and is an ideal wavelength region to collect remote sensing data for surficial studies. A new airborne system called the MODIS/ASTER (MASTER) airborne simulator, a joint development involving NASA and the U.S. Geological Survey (USGS EROS Data Center), provides the means to acquire 10 channels of TIR data (Hook, Myers, Thome, and others, 2001). MASTER data have been acquired along seven flightlines in the Front Range Urban Corridor of north-central Colorado. This study reports on the initial interpretation of data acquired along a northeast line of about 40 km from Interstate 25 to Greeley following the St. Vrain and South Platte River drainages. This urban corridor is an area of multiple use that includes agricultural land and open space, surface and ground-water bodies, sand and gravel mining, coal mining, gas and oil production, and land development. The data presented here provide surficial characterization of these areas that can be used to provide informed land-use policies for multiple use.

The diagnostic spectral features of common rock-forming minerals in the TIR occur due to the presence of the fundamental vibrational frequencies of silicate and carbonate molecules and can be detected in the spectral emissivity (the TIR equivalent of spectral reflectivity) of a material. Laboratory studies have provided fairly extensive databases (Christensen and others, 2000, among others) that can be used to analyze TIR remote sensing data. The utility of these data depends on several issues: (1) spatial resolution (pixel size), (2) spectral resolution (number of channels), and (3) data analysis methods. The MASTER instrument used in this study is an airborne system that limits the data availability to a limited number of evaluation sites (http://masterweb.jpl.nasa.gov/). The MASTER data in this study were acquired at a ground resolution of 8 m. Global satellite data are available from the Moderate Resolution Imaging SpectroRadiometer (MODIS) (http://modis.gsfc.nasa.gov/) and from the Advanced Spaceborne Thermal Emission and Reflection Radiometer (ASTER) (http://asterweb.jpl.nasa.gov/), but with a coarser spatial (MODIS: 1,000 m; ASTER: 90 m) and spectral resolution than MASTER data have. Although the spatial resolution of thermal satellite data is currently too low for most infrastructure projects, improvements are occurring rapidly. The 10-channel spectral data from MASTER represent an

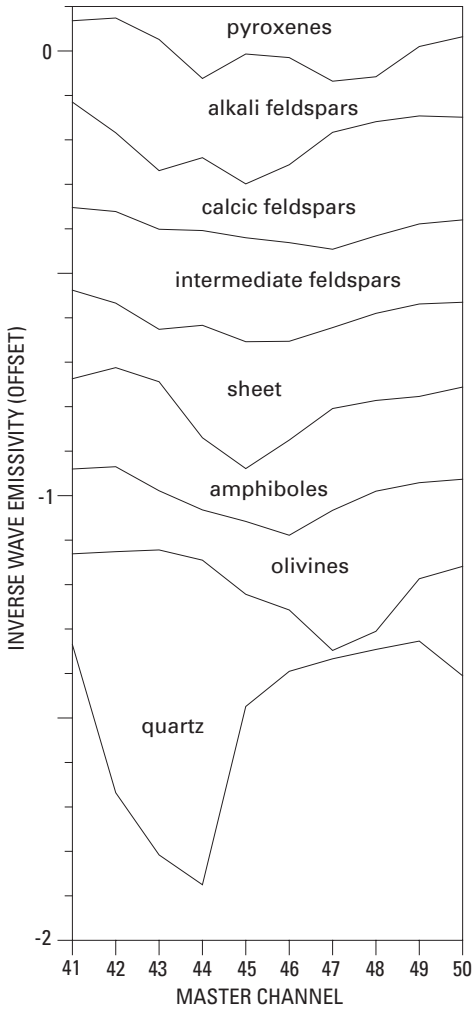

Figure 1. MASTER convolved inverse wave emissivity spectra for groups of common rock-forming minerals. The algorithm to compute the inverse wave emissivity from emissivity is described in the text. Generally the spectra are very similar in appearance to emissivity spectra because the algorithm only applies a slight tilt to the shape. This illustration is also online at http://speclab.cr.usgs.gov/PAPERS/Bulletin-2196_figs/index.html.

improvement over the 5 channels of ASTER and the 6 channels of the previous airborne Thermal-Infrared Multispectral Scanner (TIMS) system (Palluconi and Meeks, 1985), but the MASTER resolution remains considerably less than in some experimental airborne systems (such as Spatially Enhanced Broadband Array Spectrograph System (SEABASS) with >200 channels (http://www.aero.org/home.html)). Analysis techniques are also continually being developed and refined to take advantage of improvements in instrument development. In this study we employ a new algorithm that enhances spectral contrast and reduces errors introduced by temperature changes, and we display the results using an unsupervised classification algorithm. This classification algorithm has the advantage that it does not require collection of ground spectra to guide the selection of classes.

Geologic Setting

The study area is located north of Denver, Colo., on the high plains just east of the mountain front. The gently eastward sloping sedimentary terrain is cut by numerous streams and rivers that join the South Platte River throughout the area, bringing erosional detritus from the Precambrian and Tertiary rocks exposed within the interior of the Front Range mountains. The South Platte River carries this sand and gravel towards the Missouri River within its broad flood plain.

The South Platte River system in this area is composed of braided stream river channels set within a broad flood plain cut into the surrounding sedimentary bedrock, with banks containing several ages of Quaternary terraces and a pediment upland surface. Paleochannels have been cut to a depth of more than 30 m below the present channel within and near the present river course. Channel depths can reach 18 m; terrace deposits contain as much as 12 m of silt, sand, and gravel, and the pediment surfaces contain a thin layer of alluvium. South of the study area, the South Platte system is being mined for aggregate, but within the area, the gravel is too sparse for present economic recovery.

The St. Vrain River joins the South Platte near the center of the study area, transporting a coarser matrix of sand and gravel that is presently being mined in shallow aggregate open-pits within the flood plain. The sand and gravel are derived a short distance away, from granitic, volcanic, and metamorphic terranes within the mountains and from sedimentary rocks eastward of the mountain front.

Local bedrock is composed of Cretaceous age sedimentary shales and sandstones that dip gently eastward: the Fox Hills Sandstone on the west is progressively overlain by the Laramie and Arapahoe Formations. The Fox Hills Sandstone was deposited as beach sands within a deltaic environment as regional uplift shifted the inland sea shoreline eastward. The clay matrix of the Fox Hills Sandstone is principally kaolinite. Muds and sands of the Laramie followed on the emerging coastal plain where lush vegetation growth later became coal. Within the study area, clays of the Laramie Formation are principally montmorillonite. Conglomerates of the Arapahoe Formation contain Precambrian rocks derived from the uplifting Front Range.

Unconsolidated sediments overlie most of the bedrock in the study area. These Quaternary sediments occur as alluvium within stream channels, colluvium along the steeper flanks of the stream valleys, and eolian deposits of sand and silt within the upland areas. Channel alluvium generally is a variable composition of gravel, sand, silt, clay, and organic matter. Colluvium consists of sandy silt and clay, and eolian material forms sand dunes and loess deposits downwind from flood plains.

Data Sets

The primary data source for this study was the MASTER system (table 1).

See http://masterweb.jpl.nasa.gov for the central wavelength and bandwidth of the 50 channels. Thermal emissivity and temperature were obtained using channels 41–50 of the

Table 1. MASTER system.

[flight: 9/21/99]

Spectral channels: 50 (16-bit resolution). 10 TIR channels		
TIR Channel	:	Effective Wavelength
41	:	7.75 μm
42	:	8.17 μm
43	:	8.61 μm
44	:	9.05 μm
45	:	9.68 μm
46	:	10.09 μm
47	:	10.62 μm
48	:	11.32 μm
49	:	12.11 μm
50	:	12.88 μm
Instantaneous field of view: 2.5 mrad		
Ground resolution: nominally 12–50 meters (variable with altitude). 8 meters was obtained for this study.		
Total field of view: 85.92 degrees		

Table 2. AVIRIS system.

[flight: 7/1/99]

Spectral channels: 224 (16-bit resolution).
Ground resolution: nominally 20 meters (variable with altitude).
Flight altitude: 20 kilometers
Pixels/scanline: 640
Wavelengths: 0.4–2.5 micrometers

MASTER data as described in the following section. In addition channels 2, 5, 8 of the MASTER data were used to make a Color-Infrared-Composite (CIC) image for examination of vegetation cover.

Color infrared air photos (10 in. × 10 in.) were acquired simultaneously with the MASTER data. These were rolled transparencies with overlapping frames yielding full stereo coverage of the flightline.

The mica and clay identification data source for this study was the NASA–JPL Airborne Visible and Infrared Imaging Spectrometer (AVIRIS) system (table 2).

See http://aviris.jpl.nasa.gov for further specifications. A map of clay and mica minerals developed from AVIRIS data analysis was used to assist in characterizing soils. (See Clark, Swayze, and Gallagher, 1993.)

Image Setting

Line 5 of the MASTER data is centered on the St. Vrain and South Platte River drainage, extending from I-25 and the St. Vrain River on the southwest (bottom of image) to the city of Greeley on the northeast, as shown on the color-infrared-composite image (fig. 2). Features within the image include sand and gravel operations (A) that are located along the St. Vrain River at the bottom (south) of the image area, the Fort St. Vrain power plant (B) located at the confluence of the St. Vrain and South Platte Rivers—a third of the way up from the bottom of the image, and upland fields that are south of the South Platte River (C) halfway up the image on the right. A large feedlot (D) is located on the south side of the confluence of the Big Thompson and South Platte Rivers—two-thirds of the way up the image, and the city of Greeley (E) is at the top.

Methodology

The thermal radiation detected at the aircraft by the MASTER instrument can be expressed by the following:

$R_i = \tau_i\{\varepsilon_i B_i(T) + (1 - \varepsilon_i)Hsky_i\} + Hpath_i \quad i = 41,...50$

where

i - MASTER channel number

R_i - radiance detected at aircraft

τ_i - transmission in the ith channel from the ground to the aircraft

T - ground temperature

$B_i(T)$ - Planck function where $B_i(T)=c_1 e^{c_2/\lambda T}/\lambda^5(1- e^{c_2/\lambda T})$

λ is the wavelength of the ith channel, and c_1,c_2 are the radiation constants

$Hsky_i$ - hemispherical downward radiance from the sky on the ground

$Hpath_i$ - radiance from the atmosphere in the path from the ground to the aircraft

ε_i is the spectral emissivity of the ground.

If the atmospheric properties are known (τ, *Hsky*, *Hpath*) either from an atmospheric modeling program such as MODerate resolution TRANSsmittance (MODTRAN) (http://www2.bc.edu/~sullivab/soft/modtran4.html) or National Centers for Environmental Prediction (NCEP) (http://www.ncep.noaa.gov/) or from *in situ* measurements, then we have 10 equations with 11 unknowns: the 10 ε_i's and T. A number of different schemes have been proposed to resolve this dilemma, none of which is completely satisfactory. In this study we use the following method. We first estimate the ground temperature, then compute the emissivity, and lastly apply a decorrelation algorithm to minimize the error introduced by estimating the temperature (Watson, 1997). The steps are outlined as follows:

Introduce $Fcor_i=\{R_i-Hpath_i\}/\tau_i=\varepsilon_i B_i(T)+(1-\varepsilon_i)Hsky_i$.

We then compute the brightness temperature Θ_i such that $B_i(\Theta_i)=Fcor_i$ and estimate T using $Test=\max(\Theta_i)$. Note that if $\varepsilon_i=1$ for **any** i then the solution is exact.

We then use *Test* to estimate ε :

$\varepsilon est_i=\{Fcor_i-Hsky_i\}/\{B_i(Test)-Hsky_i\}$.

Lastly we decorrelate a λ^{-1} dependence from εest as follows:

Let $\varepsilon 2_i=\varepsilon est_i-\alpha/\lambda-\beta$

where $\alpha=(10*S_4-S_1*S_3)/S_2$

$\beta=(S_3-\alpha*S_1)/10$. The term $\varepsilon 2_i$ will be called the inverse wave emissivity to distinguish it from the εest_i and ε_i.

The sums S_1,S_2,S_3,and S_4 are determined:

Figure 2. MASTER color-infrared-composite image, Front Range Urban Corridor, South Platte and St. Vrain Rivers. A higher resolution image is also online at http://speclab.cr.usgs.gov/PAPERS/Bulletin-2196_figs/index.html.

$S_1=\Sigma\lambda_i$

$S_{1a}=\sum\lambda^{-1}{}_i$

$S_2=S_{1a}*10\text{-}S_1{}^2$

$S_3=\sum\varepsilon_i$

$S_4=\sum\varepsilon_i/\lambda_i$.

Finally it remains to show why decorrelating a λ^{-1} dependence from εest reduces the temperature error. Let us start with the standard equation that defines emissivity:

$\varepsilon_i=R_i/B_i(T)$

and introduce $\varepsilon o_i=R_i/B_i(T_o)$ where $T=T_o+\delta$. T_o is the estimated temperature and δ is a small error term.

Then $\varepsilon_i=R_i/B_i(T_o+\delta)$.

Now using a Taylor's expansion

$B_i(T_o+\delta)=B_i(T_o)\{1+\delta*B^{-1}\partial B/\partial T+ ....\}$

and since $\partial B/\partial T \sim -c_2*B_i(T_o)\lambda*T_o{}^2$

thus $\varepsilon_i\sim\varepsilon o_i\{1\text{-}c_2\delta/\lambda T_o{}^2\}\sim \varepsilon o_i\text{-}\gamma/\lambda$

where $\gamma=c_2\delta/T_o{}^2$.

Hence if we decorrelate a $1/\lambda$ dependence out of ε_i we remove the temperature error (at least to first order).

In this study we estimated the atmospheric parameters using the NCEP atmospheric model and then further refined these values by comparing the computed inverse wave emissivity for the Platte River with the inverse wave emissivity of tap water (Salisbury and D'Aria, 1992), using the water temperature measured at the Englewood Gage station (fig. 3). The two atmospheric models are compared in figure 4, and a plot of mean observed radiances for water and terrain are compared to fluxes computed at the aircraft for water and terrain using the refined atmospheric model, assumed temperatures, and a range of emissivities (fig. 5). The fit for water observations appears good. The fit for the ground observations is somewhat suspect at channel 41 (which appears to be low) but otherwise satisfactory. These atmospheric parameters were then used to compute a 10-channel inverse wave emissivity image (fig. 6) and a single channel estimated temperature image (fig. 7).

Classification of TIR Data

An unsupervised classification algorithm called isoclus (PCI Inc., Richmond Hill, Ontario, Canada) was then applied to the 10-channel inverse wave emissivity image in order to extract a distinct set of 15 spectral classes. Six soil classes (2, 3, 4, 6, 9, 11), one vegetation class (8), water (class 10), and several classes (1, 5, 7, 12, 13, 14, 15) associated with man-made structures were identified. An image was prepared to display the classification of soils (fig. 8) using the color coding scheme shown in table 3. The spectra of the soil, vegetation, and water classes are plotted in figure 9. The image was then examined using both field reconnaissance and information from existing maps and images, and the spectra were compared to mineral spectra (fig. 1).

Ground covered by each of the 15 derived spectral classes was studied using color-infrared air photos, color-infrared composite MASTER data (channels 8, 5, 2: RGB), field examination, the AVIRIS clay/mica image, and geologic maps to make a preliminary identification of each class's composition and spatial distribution. We also examined the use of singular value

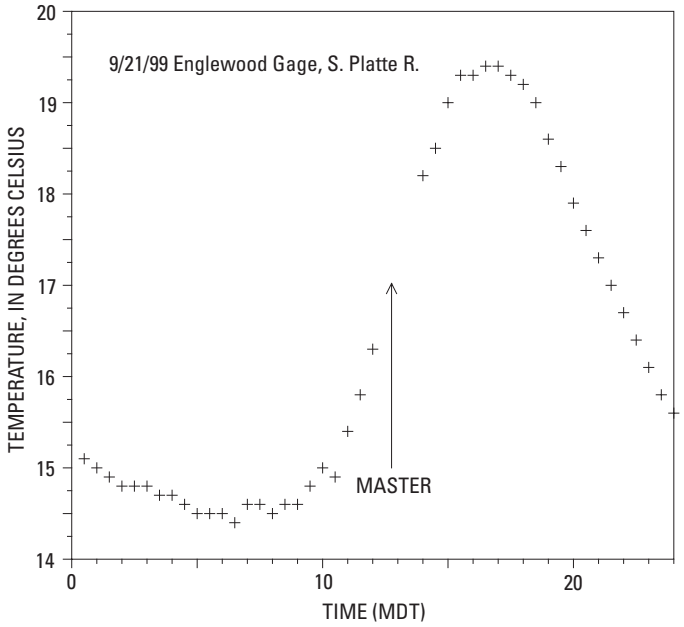

Figure 3. Temperature on the Platte River at the Englewood Gage station on the day of the overflight. The gaging station is on MASTER line 4 (not shown in report). This illustration is also online at http://speclab.cr.usgs.gov/PAPERS/Bulletin-2196_figs/index.html.

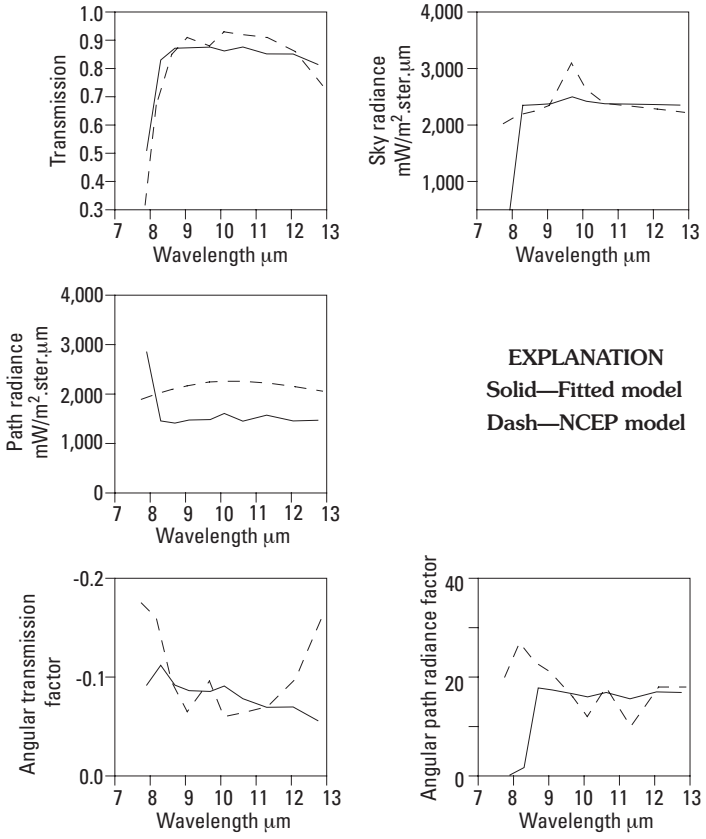

Figure 4. Model atmosphere parameter values (solid lines) derived from water radiance measurements. Dashed lines show the National Centers for Environmental Prediction model parameters for comparison. Wavelengths (x-axis) in micrometers. Significant differences between atmospheric models can be seen in the first channel in all plots. This illustration is also online at http://speclab.cr.usgs.gov/PAPERS/Bulletin-2196_figs/index.html.

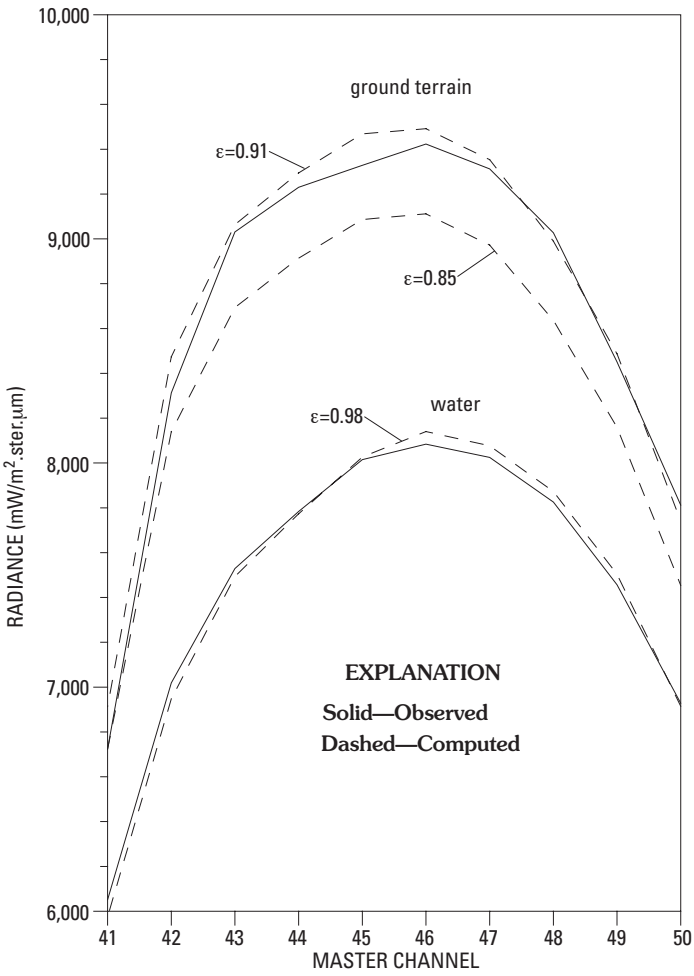

Figure 5. Observed radiance (solid) versus computed radiance (dashed) for water and ground. Computed radiance used atmospheric model (fig. 4) and emissivities indicated on the figure. This illustration is also online at http://speclab.cr.usgs.gov/PAPERS/Bulletin-2196_figs/index.html.

decomposition (Press and others, 1992), using a linear mixing model for the class 11 spectrum to estimate relative abundances as an aid to advance our understanding of material identification.

Color-infrared photography and composite MASTER images, both acquired during the MASTER flight, yielded time-dependent information on the distribution and general intensity of vegetation throughout the area, and whether the vegetation was crop, riparian, or urban landscaping. Many fields had exposed soil following fall harvest, greatly enhancing soil characterization in the autumn 1999 images. Air photos yielded spatial detail for locating test sites, and geologic maps supplied preliminary composition and geomorphic features for integration with the color-infrared images in order to make preliminary materials identification of the classes.

AVIRIS analysis used a field site to calibrate the radiance data to absolute reflectance relative to ground (Clark, Swayze, Heidebrecht, and others, 1993). Spectral analysis using the U.S. Geological Survey Tetracorder algorithm identified the clay and mica mineralogy (Clark, Swayze, and Gallagher, 1993). The results for a portion of the study are shown in the mica-clay image (fig. 10). Muscovite occurs in the rolling terrain on the northwest, muscovite with kaolinite in the sand and gravel

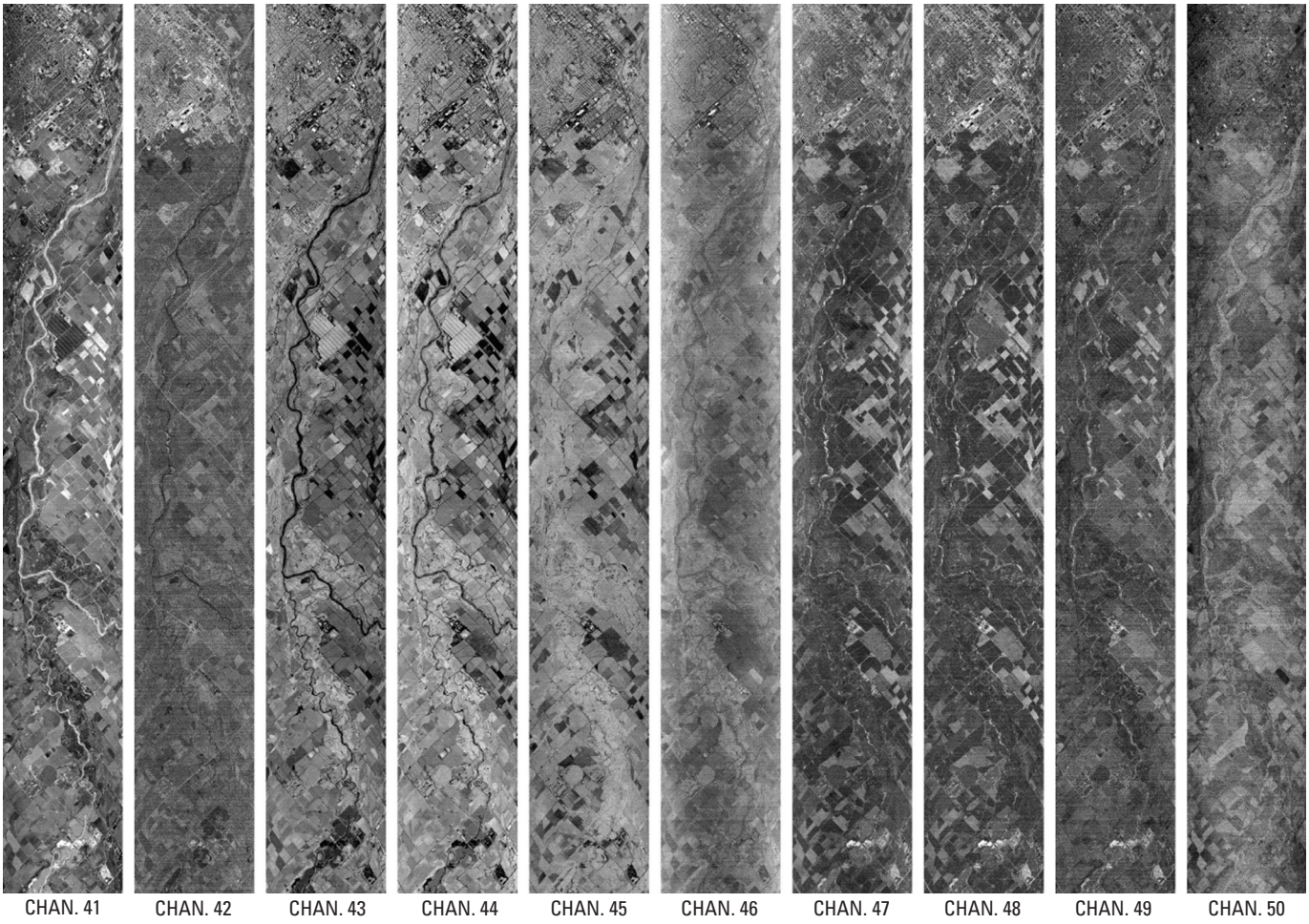

Figure 6. MASTER inverse wave emissivity images showing variation of intensities with channel number. A higher resolution image is also online at http://speclab.cr.usgs.gov/PAPERS/Bulletin-2196_figs/index.html.

quarries, montmorillonite in the upland fields, and kaolinite and muscovite southeast of the upland fields (Livo and others, 1999).

Field Examination

Mineral composition of the classes was identified through field examination. Sites were selected within homogeneous class areas and visually characterized for major quartz, feldspar, silt (particle size), clay (mineral), mica, and mafic minerals, as well as organic debris. Surface vegetation was also noted. The study area was traversed from the southwest to the northeast over a period of several days in the autumns of 2000 and 2001, when exposed ground conditions would be seasonally comparable to those during the overflight. Differences were observed that were due to changes in ground cover as a result of differences in crop plantings between the dates of data acquisition (Sept. 21, 1999) and field examination. These were identified in discussions with individual farmers. Sites were examined in relationship to bare ground as exposed during the overflight on September 21, 1999.

Generally, the soil ranged from a quartz-potassic feldspar-rich sand and gravel (class 11) to silty sand (class 9), through a silt-sand with clay (class 6), a clayey silt-sand with humus (class 4), sand-silt organic-rich clay (classes 3 and 2), and a vegetated ground (class 8). The unsupervised classification separates these soils into discrete units with arbitrary boundaries, whereas field and data examinations show a continuous variation between soil types. We discuss the classes in the order just described.

Class 11 was visually identified as being a very fine grained quartz-rich sandy soil with potassic feldspar and some muscovite and silt. The soil occurs in upland fields southeast of the South Platte River. The eolian silts and sands are derived from the St. Vrain and South Platte Rivers. The soil is very friable, does not clump well, and contains little plant detritus. This class contains coarser sand and gravel that form sandbars, sandy ground, and gravel deposits along the river drainage. It is also a constituent of asphalt road surfaces, many gravel roads, most gravel lots, and the majority of asphalt parking lots in the town of Greeley. Class 11 grades into class 9.

Class 9 was found to be a very fine grained quartz-rich silt-sand soil with some clay, potassic feldspar, and muscovite. The soil occurs in upland fields south of both the St. Vrain and South Platte Rivers along with eolian silts and sands derived from these rivers. The soil is friable, poorly clumps, and contains little plant detritus. This class represents the majority of asphalt roadways and some gravel roads. Road classification will either occur in class 9 or in class 11. Class 9 grades into class 6.

Class 6 is a very fine grained quartz-rich silt-sand soil with clay and plant humus. The soil occurs throughout the area, especially in the upland fields and in regions near riverbanks. Examined field sites have very similar soils as class 9, with the

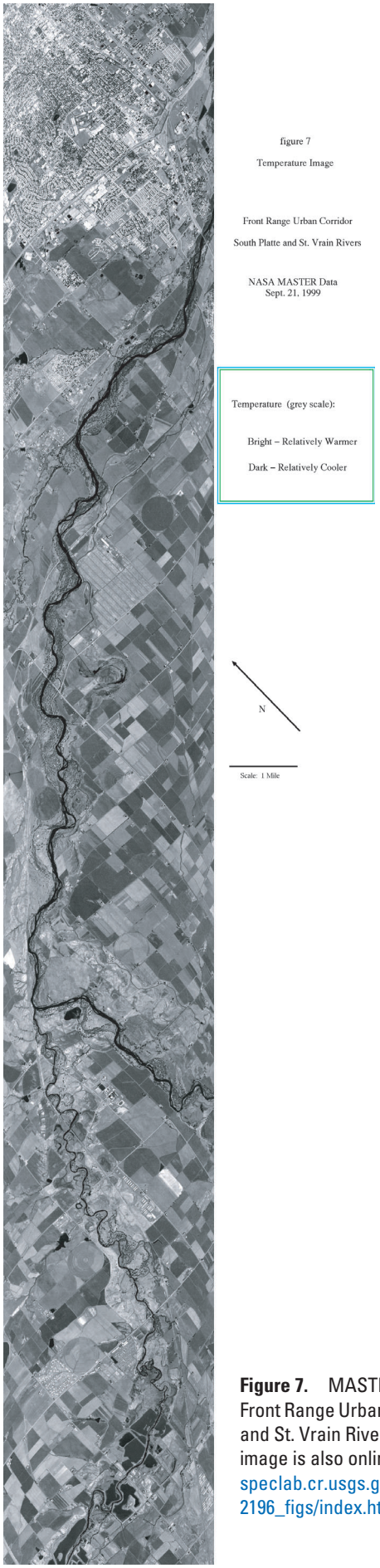

Figure 7. MASTER temperature image, Front Range Urban Corridor, South Platte and St. Vrain Rivers. A higher resolution image is also online at http://speclab.cr.usgs.gov/PAPERS/Bulletin-2196_figs/index.html.

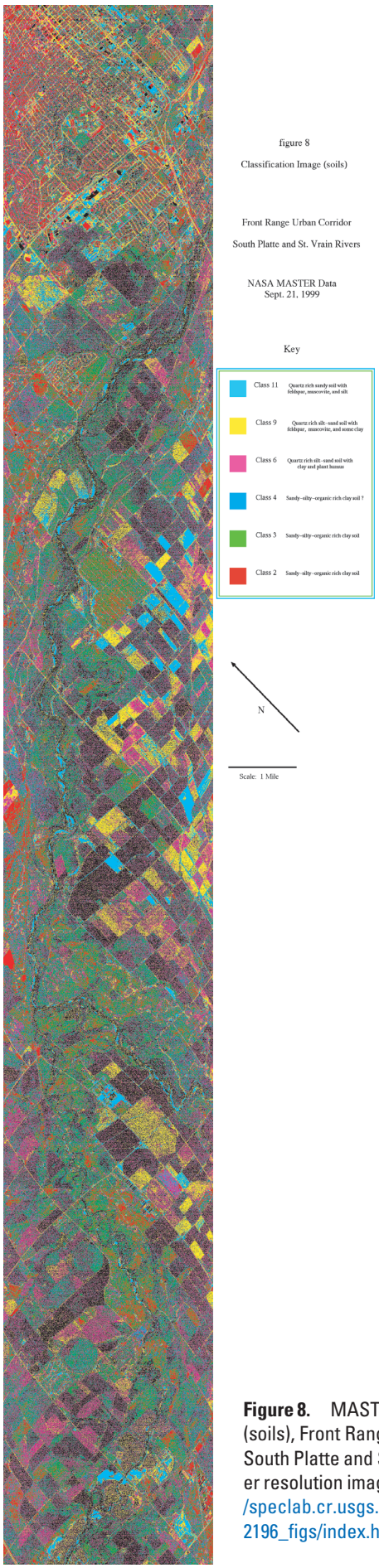

Figure 8. MASTER classification image (soils), Front Range Urban Corridor, South Platte and St. Vrain Rivers. A higher resolution image is also online at http://speclab.cr.usgs.gov/PAPERS/Bulletin-2196_figs/index.html.

Table 3. Color coding for isoclus image.

Class 2	Red
Class 3	Green
Class 4	Blue
Class 6	Magenta
Class 8	Black
Class 9	Yellow
Class 10	Black
Class 11	Cyan
Class 1,5,7,12–15	Black

addition of plant humus and clay. The soil clumps into hard dry balls. In upland fields, Class 6 occurs in fields of class 8 vegetation as bare soil between plants. In Greeley, class 6 maps streets where the spectral response appears to be integrated between asphalt, roofs, and trees. Class 6 grades into class 4.

Class 4 was not examined independent of class 3 in the field but was observed to grade into class 3 on the classification image.

Class 3 is a sandy-silty-organic-rich clay soil that occurs as over-bank fill in flood plains, riverbanks, and stockyards, and as soil in turf farms and irrigated grass landscaping. This class is the dominant soil in the riparian areas of the St. Vrain and Platte River drainages and has open canopy vegetation that may explain the upturn in channel 50 similar to class 8 vegetation spectra (fig. 9). Class 3 grades into class 2.

Class 2 is a sandy-silty-organic-rich clay soil very similar to class 3. It occurs in areas that are marshy during part of the year, such as flood plains, drainage ditches, and irrigated fields, where trees, rushes, and other high-chlorophyll plants are abundant. In Greeley, roofing materials and some fields were identified in class 2.

Class 8 contains abundant vegetation, generally closed canopy cover, occurring in the upland fields as crops and trees and in the city of Greeley as trees and other landscaping.

Class 10 is water and water-bearing soil, including the South Platte and St. Vrain Rivers, ponds, and marshes with exposed water. Fields that most likely were heavily irrigated were also mapped, but not field checked.

Examination of Spectra

In the thermal infrared wavelength region, minerals emit electromagnetic radiation with diagnostic spectral shapes caused by molecular vibrations. The laboratory spectra for quartz, olivines, amphibolites, sheet minerals (mica, clay, and chlorite), feldspars, and pyroxenes are shown (convolved to MASTER wavelengths and converted to inverse wave emissivities) in figure 1. Quartz has a strong asymmetric minimum centered at channel 44, with steep slopes, a broad maximum at the longer wavelengths past the minimum, and a downturn at channel 50. The sheet minerals (mica, clay, and chlorite) generally have a

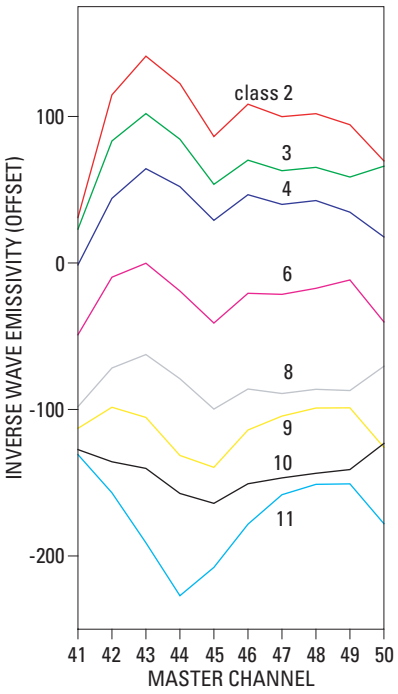

Figure 9. Inverse wave emissivity spectra of unsupervised soil and vegetation classes. Class spectra were defined by the unsupervised classification algorithm. This illustration is also online at http://speclab.cr.usgs.gov/PAPERS/Bulletin-2196_figs/index.html.

maximum at channel 42, a minimum at channel 45, and a spectrum that flattens at the longer wavelengths. Feldspars have flattened spectra with multiple minimums: at channels 43 and 45 for alkali feldspars, at channels 43 and 45-46 for intermediate feldspars, and at channels 43 and 47 for calcium feldspars. Pyroxenes have minimums at channels 44 and 47-48 whereas amphiboles have a minimum at channel 46. Olivines have an asymmetric minimum centered at channel 47 and shoulders at channels 45 and 48.

Eight spectral classes proved useful in characterizing the most abundant surface materials within the MASTER data. Six soil spectral classes (classes 2, 3, 4, 6, 9, and 11: red, green, blue, magenta, yellow, and cyan), the vegetation class (class 8), and the water class (class 10) have distinct spectral emissivity characteristics that can be related to their material content. Comparisons of these distinct features with laboratory mineral spectra help explain the features and their meaning in terms of material composition.

We begin with an empirical examination of the class spectra (fig. 9) to discover the most significant features. The top six spectra in figure 9 (classes 2, 3, 4, 6, 8, and 9) have a similar shape with a maximum at channel 43, a minimum at channel 45, and some variation in the shape at wavelength channels greater than 47.

Class 11 (fig. 9), distinctly different from the other classes, exhibits a sharp decrease to the minimum at channel 44, a rise to a maximum centered at channels 48 and 49, and a strong

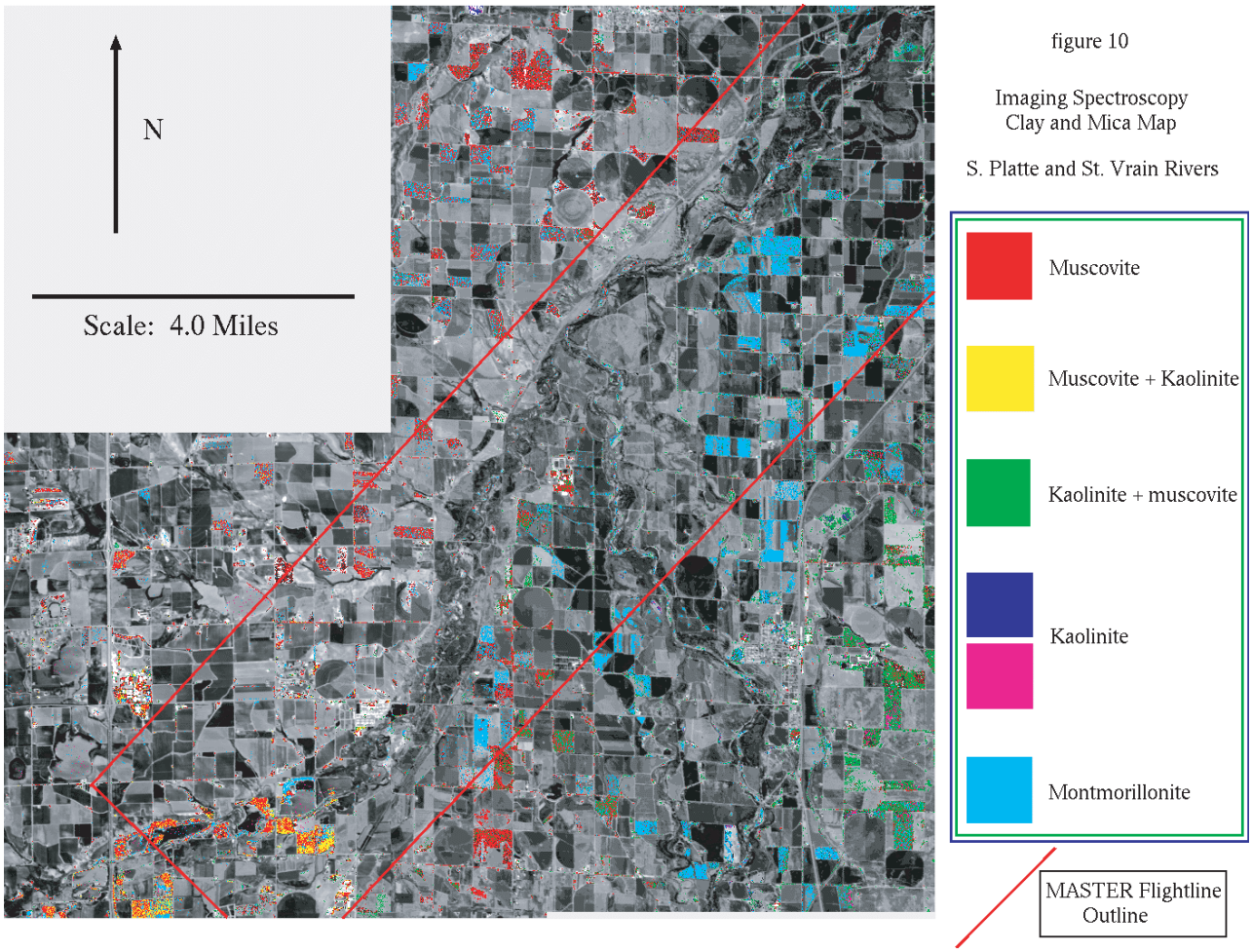

Figure 10. AVIRIS imaging spectroscopy clay and mica map, South Platte and St. Vrain Rivers. A higher resolution image is also online at http://speclab.cr.usgs.gov/PAPERS/Bulletin-2196_figs/index.html.

downturn at channel 50. This spectrum is similar to the quartz spectrum seen in figure 1. Class 9 has a shape intermediate between class 11 and class 6 with a broad minimum at channels 44 and 45. This suggests a quartz-rich soil with mica and (or) clay. The channel 45 minimum displayed by the other soil classes (2, 3, 4, and 6) corresponds to the minimum that can be observed in the sheet mineral spectrum (fig. 1) and indicates the presence of mica and (or) clay minerals. Class 4 (which was lumped with class 3 in the field investigation) appears to differ only at channel 50, suggesting that the difference between the two classes is due to a greater vegetation component in class 3 (fig. 9).

The spectral character at the higher channels (fig. 9) appears quite diagnostic for material classification. Classes with a downturn at channel 50—2, 4, 6, 9, and 11—generally have low vegetation cover while classes with an upturn—3, 8, and 10—are soil with grasses and other open canopy vegetation (class 3), closed canopy vegetation (class 8), and water (class 10), based on field observation. Sandier soils (classes 6, 9, and 11) have a positive slope at the longer wavelength channels (45–49) whereas the more clay rich soils (classes 2, 3, and 4) have a negative slope (fig. 9). Class 10, which we associate with water, has a flattened spectrum. The water spectrum has a significant upturn at channel 50 that is not inconsistent with vegetation (mixed water-vegetation pixels).

MASTER soil class spectral features are formed from a combination of mineral spectra. An example is the sand and gravel class (class 11: cyan). Field examination of material in this class revealed a quartz-rich sandy soil with potassic feldspar and some muscovite and silt. Thus we expect to find a combination of these mineral spectra in the spectra of the class. A model with a linear combination of the spectra for the minerals quartz, potassium-feldspar, and clay (fig. 11) was least squares fitted using single value decomposition to a subset of class 11 representing the sand and gravel quarry near the bottom of the image. Figure 12 shows a comparison between the fit and the observed spectra. The abundances of the fitted spectrum: 55 percent quartz, 20 percent potassium-feldspar, 23 percent clay (and (or) mica and (or) chlorite), with a 41 percent spectral scaling (flattening) factor correlated well with the field-examined quartz arkose with muscovite, a trace of mafic minerals, and little clay. Results of linear spectral mixing of minerals for the other classes

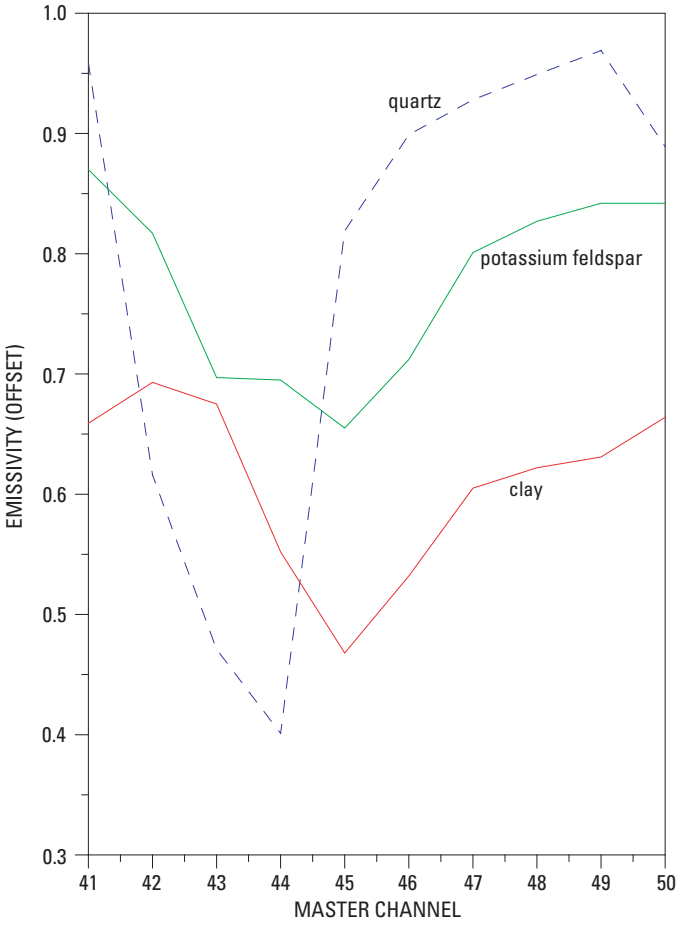

Figure 11. MASTER convolved emissivity spectra for quartz, potassium feldspar, and clay. The feldspar and clay spectra are averages computed from several mineral spectra. This illustration is also online at http://speclab.cr.usgs.gov/PAPERS/Bulletin-2196_figs/index.html.

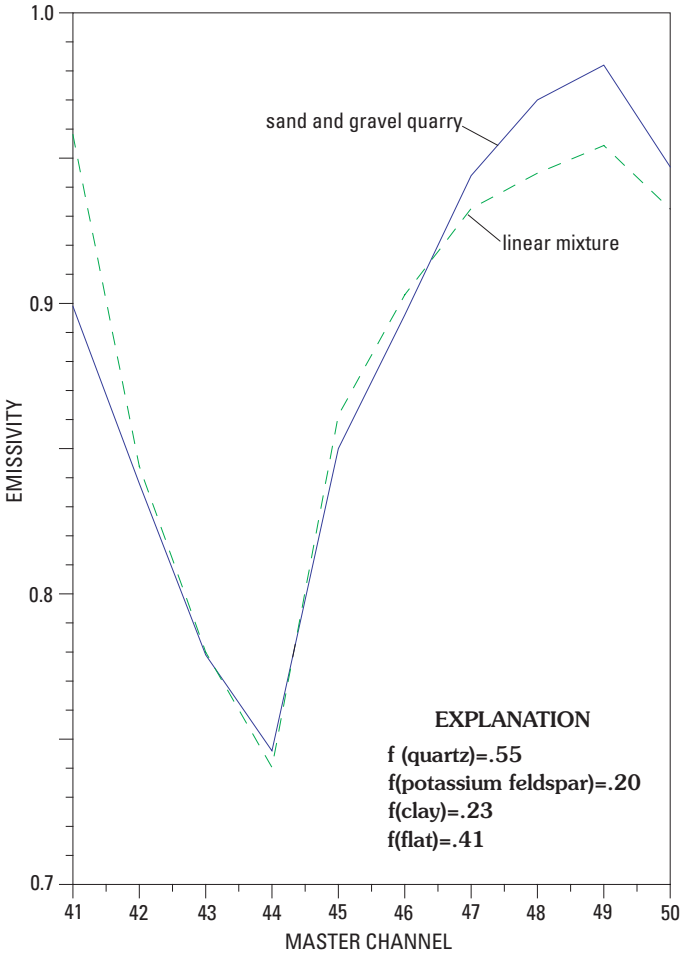

Figure 12. Comparison between observed MASTER spectrum from an area in a sand and gravel quarry with a linear mixture of laboratory spectra. (See fig. 11.) The fractions were derived using a single value decomposition algorithm. This illustration is also online at http://speclab.cr.usgs.gov/PAPERS/Bulletin-2196_figs/index.html.

were not conclusive. For the other classes, no models with a linear combination of mineral spectra agreed with observed soil mineralogy.

Distribution and Analysis of Classes Within the Flightline 5 Image

The sand and gravel operations (A: fig. 2) along the St. Vrain River were classified with the MASTER data as class 11 (cyan). Class 11—quartz-rich sand quarries (cyan) are fringed by class 9—quartz-rich silt-sand soil (yellow) and contain class 9 material bearing roads. Field verification (which used these quarries as one of several sites for defining class 11 mineralogy) showed that the extracted sand and gravel was a quartz-rich potassic-feldspar arkose with muscovite and a trace of mafic minerals, and little clay. Quartz dominates the mineral grains, and the site has a very strong quartz absorption feature in the MASTER data. The roads and fringing areas map as having some clay with the quartz sands (fig. 8).

The Fort St. Vrain power plant area (B: fig. 2) mapped as quartz-rich sands (cyan: class 11) that were field verified as quartz-rich gravel. The main buildings are surrounded by gravel lots where fill was hauled to the site. Likewise, dirt roads in the area are quartz-rich gravel that map with varying amounts of clay (cyan and yellow: classes 11 and 9). Other introduced quartz-rich gravel in the region, seen as squares with a few pixels on each side (cyan: class 11), are gravel lots used for power substations. The AVIRIS image (fig. 10) shows muscovite in the gravel.

Upland fields (C: fig. 2) mapped as a group of sandy soils, ranging from quartz-rich sandy soil (cyan: class 11), to quartz-rich silt-sand (particle size) soil with some clay mineral (yellow: class 9), and to quartz-rich silt-sand soil with clay and plant humus (magenta: class 6). Class 4, silt-sand-clay (blue), is interwoven throughout class 6, especially near boundaries with class 3 (green). The soils appear to have a natural variability in silt

and clay content. Eolian sands and silts were derived from the South Platte River. Field investigations show that the soils have a continuous range in composition, but the unsupervised classification algorithm statistically places the soils into discrete classes. Feathering of the edges of adjacent classes shows this effect. Variation of composition between fields can be attributed to farmers' amending their fields by plowing under crop remains and fertilizing fields with manure. The change in clay and humus is seen in the class spectra, with longward shift in the spectral minimums, from quartz-feldspar absorption features, to clay absorption features. Progressive flattening of the spectra longward of the main absorption features occurs with increasing clay and humus content. The AVIRIS image shows montmorillonite clay as the dominant sheet mineral.

Soils from the large feedlot and a smaller feedlot (D: fig. 2) 3 km to the east mapped as sandy-silty-organic-rich clay (green and red: classes 3 and 2) in the MASTER soil classification image (fig. 8). Field checking verified the organic composition of the soil. No growing vegetation existed within the stockyards. Moisture in the soil may suppress spectral maximums but will not change the overall characteristics of the class spectra.

The city of Greeley (E: fig. 2) contains all classes of materials. The sand classes mapped mainly as various types of asphalt whereas the three clay classes mapped clay-rich ground and roofing material. The quartz-rich sands class (cyan: class 11) occurs as asphalt road surfaces and as the majority of asphalt parking lots. Abundant quartz gravel in this pavement was apparent during field checking. The quartz-rich silt-sand soil with some clay class (yellow: class 9) comprises the majority of asphalt roadways. This pavement also has quartz gravel, though the difference between the class 11 and this class variety of asphalt was not studied. A third class of asphalt occurs with class 6 (magenta), a quartz-rich silt-sand soil with clay and plant humus class. Class 6 occurs on streets where the spectral response appears to be integrated among asphalt, roofs, and trees.

The three clay classes within Greeley (classes 4, 3, and 2: blue, green, and red) mapped a more diverse group of materials. Generally, classes 4 and 3 mapped silt-clay soils in areas of irrigated grass landscaping, whereas class 2 mapped some fields, and roofing materials on residential houses and businesses, particularly on the west side of the image area. Exactly what materials in the roofs correlate with class 2 is unclear.

Flood plains of the South Platte and St. Vrain Rivers mapped as sandy-silty-organic-rich clay throughout the drainage (blue, green, and red: classes 4, 3, and 2); the associated river channels and eroded ground mapped as quartz-rich sands (cyan: class 11). Throughout the flood plains, the soils appear to be a consistent mixture of the three classes. Likewise, the channel sands remain homogeneous throughout their lengths within the MASTER classified soil image. Sand and gravel occur under the well-developed organic-rich soil and are visible in eroded areas and river bottoms where burrowing animals have brought sand to the surface. Whereas MASTER mapping classified sheet silicate minerals within the area, AVIRIS mapping identifies the sheet silicate minerals as muscovite within the sand and gravel and muscovite and kaolinite within mined land. Vegetation prevented the over-bank soil from being identified using AVIRIS data.

Riverbanks and rolling terrain mapped primarily as quartz-rich silt-sand soil with clay and plant humus (magenta: class 6) with class 4 (blue) and class 3 (green) scattered throughout. Generally, these areas field checked as silty soil with natural dryland vegetation. The AVIRIS image shows muscovite as the dominant sheet mineral.

Summary

MASTER data were processed using an algorithm to compute the inverse wave emissivity. The processing employed an atmospheric model derived from an existing regional model by using the observed MASTER radiance observations of the South Platte River and ground radiances computed using water temperature measurements. An unsupervised classification algorithm was applied to the results to identify a spatially unique set of spectral classes. These data were then analyzed by field examination and comparison with other maps and images and mineral spectral databases.

Quartz-rich sands were directly identified using their spectral signature, as were sand and gravel mines, sandbars, and sandy soil (as well as asphalt and gravel lots). Analysis of a MASTER spectrum of the sand and gravel operation (labeled A, fig. 2) led to discovering a spectral mineral mixture of quartz, feldspar, and sheet silicate minerals that agreed with the field observations.

Data spatial resolution allowed fine structures such as sandbars within the river channels, dirt roads, and small gravel lots to be seen. Eolian quartz-rich sands derived from the river channels have been carried by the prevailing wind to form soils in fields south of the South Platte and St. Vrain Rivers. The identification of eolian sands might be used to locate river segments with abundant sands that may indicate sand and gravel deposits of economic interest.

A range of soils with varying amounts of quartz, silt, clay, and plant humus are mapped in the upland farm fields south of the South Platte River. The quartz and clay abundance could be qualitatively estimated in these soils by examination of their spectral features. Emissivity minimums at channels 44, 45, and 50, maximums at channels 43 and 48–49, and spectral slopes were used to coarsely characterize quartz and clay abundances. Quality of the quartz sands is indicated by these spectral responses and might be used to help evaluate the sand's desirability for construction, farming, or stability from erosion.

Two river bottom soils capping river fill were mapped. These sand-silt-organic-rich clay soils are characteristic of the flood plains of both rivers. One soil comprises over-bank deposits; the other soil is generally found in areas that are marshy during part of the year. The two soils have very similar spectra with the exception of the last channel. These clay-rich soils are distinctly different from the upland sandy soils, in both geomorphology and spectral character, with a very flattened spectral response longward of channel 45. This type of soil could possibly be used in other areas to indicate conditions permissible for sand and gravel operations.

The results of this study indicate that MASTER thermal data provide a useful tool for characterizing the composition and quality of materials that commonly occur in areas useful for infrastructure resources. Satellite data of similar spectral and spatial resolution could be used to characterize and map soil mineralogy and physical parameters over large geographic areas.

References Cited

Clark, R.N., Swayze, G.A., and Gallagher, A.J., 1993, Mapping minerals with imaging spectroscopy, *in* Scott, R.W., Jr., Detra, P.S., and Berger, B.R., eds., Advances related to United States and international mineral resources—Developing frameworks and exploration technologies: U.S. Geological Survey Bulletin 2039, p. 141–150.

Clark, R.N., Swayze, G.A., Heidebrecht, K.B., Goetz, A.F.H., and Green, R.O., 1993, Comparison of methods for calibrating AVIRIS data to ground reflectance, *in* Green, R.O., ed., Summaries of the fourth annual JPL airborne geosciences workshop, Volume 1: AVIRIS workshop, Jet Propulsion Laboratory Publication 93-26, p. 31–34.

Christensen, P.R., Bandfield, J.L., Hamilton, V.E., Howard, D.A., Lane, M.D., Piatek, J.L., Ruff, S.W., and Stefanov, W.L., 2000, A thermal emission spectral library of rock-forming minerals: Journal of Geophysical Research, v. 105, p. 9735–9739 (available online at URL http://speclib.jpl.nasa.gov/).

Hook, S.J., Myers, J.J., Thome, K.J., Fitzgerald, M., and Kahle, A.B., 2001, The MODIS/ASTER airborne simulator (MASTER)—A new instrument for earth science studies: Remote Sensing of the Environment, v. 76, Issue 1, p. 93–102.

Livo, K.E., Hummer-Miller, Susanne, and Knepper, D.H., Jr., 1999, Surface mineral composition of selected flood plains within the Colorado Front Range Urban Corridor mapped using remotely sensed data, *in* Bon, R.L., Riordan, R.F., Tripp, B.T., and Krukowski, S.T., eds., Proceedings of the 35th Forum on the Geology of Industrial Minerals—The Intermountain West Forum 1999: Utah Geological Survey Miscellaneous Publication 01-2, p. 240–241.

Palluconi, F.D., and Meeks, G.R., 1985, Thermal infrared multispectral scanner (TIMS)—An investigator's guide to TIMS data: Jet Propulsion Laboratory Publication 85-32.

Press, W.H., Teukolsky, S.A., Vellerling, W.T., and Flannery, B.P., 1992, Numerical recipes in Fortran 77, Second Edition: Cambridge University Press, section 2.6, p. 51–63.

Salisbury, J.W., and D'Aria, D.M., 1992, Emissivity of terrestrial materials in the 8-14 micrometer atmospheric window: Remote Sensing of the Environment, v. 42, p. 83–106.

Watson, Ken, 1997, Three algorithms to extract spectral emissivity information from multispectral thermal data and their geologic applications: First JPL Workshop on remote sensing of Land Surface Emissivity, Pasadena, Calif., May 6–8, 1997.